Magnetic order and exchange coupling in the frustrated diamond-lattice antiferromagnet $MnSc_2Se_4$

K. Guratinder[*,†]
Laboratory for Neutron Scattering and Imaging, Paul Scherrer Institute, CH-5232 Villigen, Switzerland and Department of Quantum Matter Physics, University of Geneva, CH-1211 Geneva, Switzerland

V. Tsurkan and L. Prodan
Experimental Physics V, University of Augsburg, D-86135 Augsburg, Germany and Institute of Applied Physics, str. Academiei 5, MD 2028, Chisinau, Republic of Moldova

L. Keller, J. P. Embs, and F. Juranyi
Laboratory for Neutron Scattering and Imaging, Paul Scherrer Institute, CH-5232 Villigen, Switzerland

M. Medarde
Laboratory for Multiscale Materials Experiments, Paul Scherrer Institute, CH-5232 Villigen, Switzerland

Ch. Rüegg
Neutrons and Muons Research Division, Paul Scherrer Institut, CH-5232 Villigen, Switzerland and Department of Quantum Matter Physics, University of Geneva, CH-1211 Geneva, Switzerland

O. Zaharko[†]
Laboratory for Neutron Scattering and Imaging, Paul Scherrer Institute, CH-5232 Villigen, Switzerland

(Received 10 November 2021; revised 23 March 2022; accepted 25 March 2022; published 19 May 2022)

We report the magnetic properties of the *A*-site spinel compound $MnSc_2Se_4$. The macroscopic magnetic measurements uncover successive magnetic transitions at $T_{N1} = 2.04$ K, followed by two further transitions at $T_{N2} = 1.8$ K and $T_{N3} = 1.6$ K. Neutron powder diffraction reveals that both $T_{N2} < T < T_{N1}$ and $T < T_{N3}$ orders are associated with the propagation vector $k = (3/4, 3/4, 0)$, while the magnetic structures are collinear amplitude modulated and helical, respectively. Using neutron powder spectroscopy we demonstrated the effect of substitution of S by Se on the magnetic exchange. The energy range of the spin-wave excitations is suppressed due to the chemical pressure of the X ion in $MnSc_2X_4$ (X = S, Se) spinels.

DOI: 10.1103/PhysRevB.105.174423

I. INTRODUCTION

The A sites of the AB_2X_4 spinel compounds constitute a bipartite diamond lattice [1–5], where the frustration appears due to the competition of the nearest-neighbor coupling J_1 (NN), next-nearest-neighbor coupling J_2 (NNN) [1,5] (see Fig. 1), or due to higher-order exchange terms. In addition to the magnetic frustration, anisotropy plays a crucial role in the selection of the magnetic ground state in the *A*-site magnetic spinels [6,7]. The well-known member of this family is $MnSc_2S_4$, where $S = 5/2$ Mn^{2+} ions form a spiral spin-liquid state [8]. Recently, $MnSc_2S_4$ has also been found to possess a promising field-induced antiferromagnetic skyrmion lattice state [7].

In an archetypal cubic spinel $A^{2+}B_2^{3+}X_4^{-2}$, the A^{2+} ions occupy the tetrahedral sites and form a diamond lattice and the B^{3+} ions stay in the octahedral sites forming a pyrochlore lattice. The diamond lattice of the *A*-site spinel with magnetic ions at the $(0, 0, 0)$ and $(1/4, 1/4, 1/4)$ positions constitutes two interpenetrating face-centered-cubic (fcc) lattices. The three most relevant exchange paths, namely J_1, which couples ions between two fcc lattices, J_2, that couples ions within same fcc lattice, and J_3 are shown in Fig. 1. The diamond lattice of the *A*-site magnetic spinel has four J_1 and twelve J_2 interactions.

The magnetic diamond lattice with only J_1 is not frustrated and results in a collinear antiferromagnetic order. However, the magnetic interactions become frustrated when J_2 is antiferromagnetic and significant, which suppresses the long-range collinear antiferromagnetic ordering and results in a spin-liquid ground state. Theoretical calculations [1] showed that if the ratio of J_2/J_1 is $0 \leqslant J_2/J_1 \leqslant 1/8$, the ground state will be a collinear Néel antiferromagnet, while for $J_2/J_1 > 1/8$, it results in a degenerate spiral spin-liquid ground state.

A-site spinels offer a multitude of exotic and novel properties to be explored experimentally as well as theoretically. Up to now, *A*-site spinels have unveiled a broad range of

[*]Present address: Max Planck Institute for Solid State Research, 70569, Stuttgart, Germany.
[†]Corresponding authors: g.kaur@fkf.mpg.de; oksana.zaharko@psi.ch

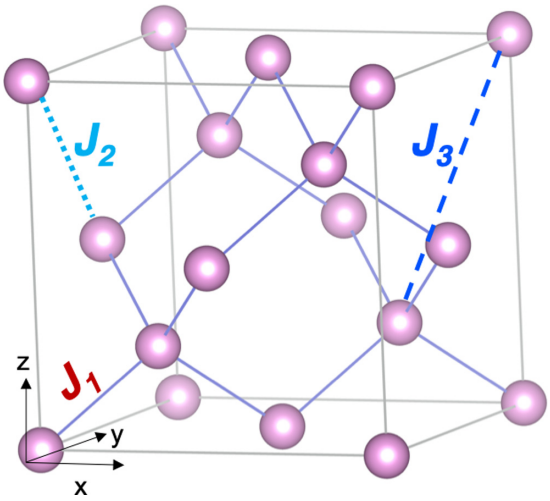

FIG. 1. The diamond lattice composed of A sites of the spinel AB_2X_4. The first-, second-, and third-neighbor exchange interaction terms are denoted by J_1, J_2, and J_3.

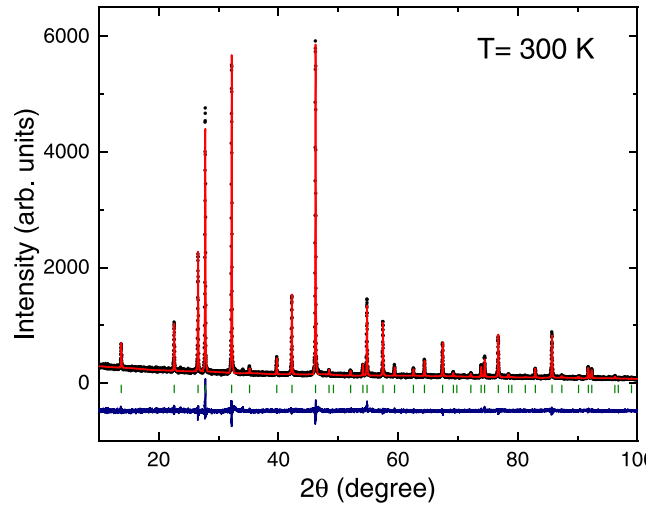

FIG. 2. Room-temperature powder x-ray diffraction pattern and the Rietveld refinement. The experimental profile is shown by black circles, the calculated profile by the red solid line, and the difference between the calculated and the observed pattern is indicated by the blue solid line. The green vertical bars indicate the expected Bragg peak positions.

interesting materials, such as cobaltates Co_3O_4 and $CoRh_2O_4$ [9], the aluminates MAl_2O_4 with $M = Mn$, Co [10–14], and the thiospinel $MnSc_2S_4$ [15]. Among them, Co_3O_4, $CoRh_2O_4$, and $MnAl_2O_4$ exhibit a comparatively lower frustration index, $f = |\Theta_{CW}|/T_N = 3.7$, 1.2, and 3.6, respectively, lying deep in the Néel phase. Recently, $MnSc_2S_4$ with $f = 10$ realized an exotic spiral spin-liquid state [1,16–18]. Extending the further insight into the intriguing physics of $MnSc_2X_4$ systems, here we show that $MnSc_2Se_4$, a sister compound, is a next candidate to host similar exotic magnetic states such as spiral spin liquids, skyrmions, and vortices.

In the present paper, we tune the J_2 and J_1 exchange couplings with chemical pressure by replacing S with Se. Broadly, the magnetic properties of the Se analog resemble those of $MnSc_2S_4$ but the exchange interaction parameters are significantly smaller. Using macroscopic magnetic measurements and neutron scattering on polycrystalline $MnSc_2Se_4$, an unconventional multistep magnetic ordering has been revealed. We found a reduction of the Curie-Weiss (Θ_{CW}) and the ordering (T_N) temperatures, and a reduced energy range of spin excitations on replacing S by Se. Motivated by the findings in $MnSc_2S_4$ [7] we decided to introduce the perturbations in the spin Hamiltonian and to the magnetic properties via exchange interactions. A famous example of such effects is the spinel family AB_2X_4, with $B = Cr$, where the size of the A- and X-site ions influences the magnetic exchange interactions [19]. Here, the Cr d t_{2g} states and X p states are important for the formation of Cr magnetic moments and for the exchange between them. All the members of the ACr_2X_4 family reveal a clear preference to ferromagnetism on increasing the size of the X-site ion.

Theoretical studies of the effective exchange couplings in these spinels were primarily based on the Goodenough-Kanamori rules of the superexchange mechanism. In brief, these rules predict the sign and the strength of the interatomic spin-spin interactions controlled by a superexchange mechanism. As the distance between the atoms varies, the ensuing change in exchange couplings is expected. In our case, when S is replaced by a larger Se, the lengths of both Mn-X ($X = S$, Se) and Sc-X bonds increase, which eventually leads to a change of J_3, J_2, and J_1. In the present investigation we explore a method to engineer such tuning of J's in the $MnSc_2Se_4$ system.

II. SAMPLE CHARACTERIZATION

The polycrystalline sample was prepared by solid-state synthesis from high-purity elements by several repeating synthesis at 1000 °C. To exclude the formation of oxide impurities, all technological procedures (mixing, pressing, and loading of materials in ampoules) was done in an Ar box with a residual concentration of O_2 and H_2O of less than 1 ppm. The obtained powder sample is characterized by standard powder x-ray diffraction using Cu $K\alpha_1$ radiation, and the Rietveld refinement using FULLPROF software [20] of the obtained data confirmed the normal cubic spinel structure without the presence of any secondary phases (Fig. 2). The room-temperature lattice constants are $a = b = c = 11.0887(1)$ Å and the refined fractional coordinate of the Se atom on the 32e site is $x = 0.2568(1)$.

The magnetization data were recorded using a commercial superconducting quantum interference device (SQUID) magnetometer (Quantum Design MPMS) with a ^{3}He cryostat. The magnetic susceptibility data measured in the low-temperature regime (450 mK $\leqslant T \leqslant$ 4.5 K) indicate three transitions at $T_{N1} \sim 2$ K, $T_{N2} \sim 1.8$ K, and $T_{N3} \sim 1.6$ K, as shown in Fig. 3(a).

These magnetic transitions get less prominent with applied magnetic field and they are no longer discernible above 4 T. The inverse susceptibility data fitted to a Curie-Weiss law in the paramagnetic regime above 50 K, gave $\Theta_{CW} = -18.4(1)$ K. The magnetic susceptibility data measured in a broad temperature range (1.8 K $\leqslant T \leqslant$ 400 K) are shown in Fig. 3(b), and Fig. 3(c) refers to the inverse susceptibility data.

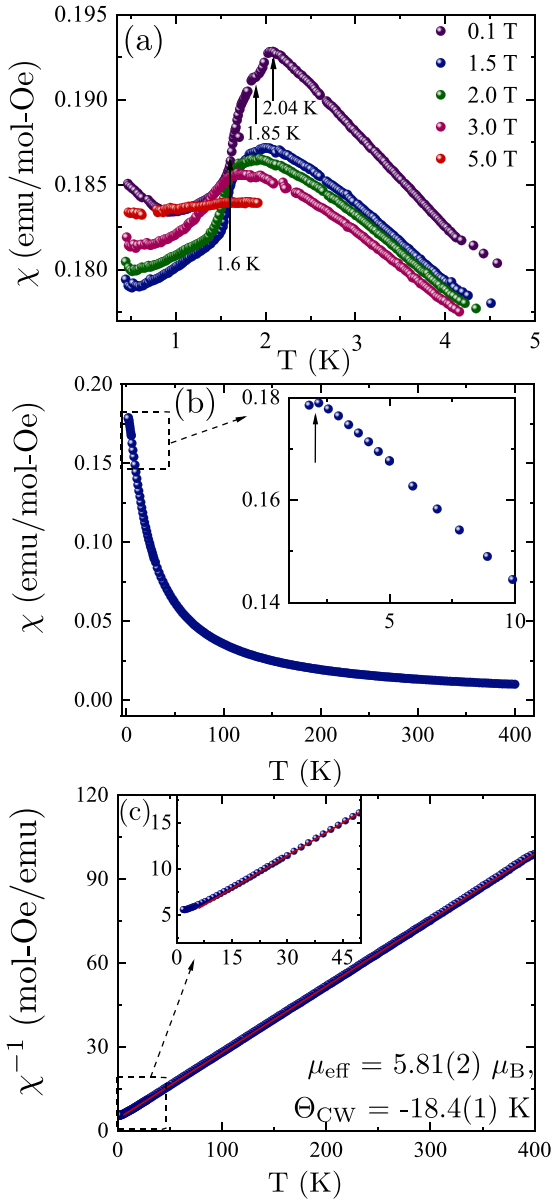

FIG. 3. (a) Magnetization vs temperature of $MnSc_2Se_4$ measured at 0.1, 1.5, 2, 3, and 5 T showing multiple transitions. (b) Magnetic susceptibility at $H = 1$ T with the inset indicating the transition around 2 K. (c) Inverse susceptibility with the extracted Curie-Weiss constant Θ_{CW} and an effective moment. The inset refers to the deviation from the Curie-Weiss fit close to $|\Theta_{CW}| \sim 18.4$ K.

The effective moment $\mu_{eff} = 5.81(2)\mu_B$ extracted from this fit is close to the spin-only value of $5.92\mu_B$ for Mn^{2+} ($3d^5$) $S = 5/2$. The frustration index, $f = |\Theta_{CW}|/T_N \sim 9.0$, reflects the presence of significant frustration. The deviation from the Curie-Weiss behavior below 18.4 K [Fig. 3(c) inset] infers the presence of short-range magnetic correlations [21,22].

III. MAGNETIC CORRELATIONS FROM NEUTRON DIFFRACTION

Neutron powder diffraction patterns were collected on DMC, SINQ at PSI with an incident neutron wavelength of 2.46 Å. The experiment was performed with ~4.58 g of a polycrystalline sample, which was inserted into an air-sealed vanadium sample can (V can) with an inner diameter of 8 mm. To obtain the desired low temperatures up to 1.3 K, we have used a He cryostat with a roots pump. The patterns have been recorded at several temperatures that were chosen based on the results from the macroscopic magnetization measurements.

The obtained diffraction data have been analyzed using the FULLPROF program [20]. First, the nuclear structure was refined against the data taken at 20 K, which confirms the space group $Fd\bar{3}m$ (227) and lattice constants $a = b = c = 11.0873(6)$ Å. Figures 4(a) and 4(b) show the difference patterns obtained by subtracting the data taken at 20 K (uncorrelated state) from the data at low temperatures (correlated state), here the low temperatures refer to 1.25 and 1.7 K. They reveal magnetic Bragg peaks and a diffuse bump at $2\theta = 12°$–$14°$. We refined the Bragg peaks in difference data with the propagation vector $k = (3/4, 3/4, 0)$ using the helical and the amplitude modulated models developed for $MnSc_2S_4$ [8]. The diffuse scattering was incorporated into the background for these refinements. The different quantities, commonly termed as agreement factors, are calculated to identify the quality of the fit.

From our refinement of the 1.25–20 K difference data, we obtained, for the helical model magnetic Bragg factor $R_B = 10.3\%$, profile factor $R_p = 5.9\%$, weighted profile factor $R_{wp} = 6.8\%$, and the goodness of fit $\chi^2 = 2.6$. This model fits very well near $T = 1.25$ K but fails to converge for higher temperatures. Then the amplitude modulated model is used to describe the data and we conclude that this model is fitting well at and above $T = 1.7$ K. The agreement factors are $R_B = 18\%$, $R_p = 5.67\%$, $R_{wp} = 6.83\%$, and $\chi^2 = 2.82$. In the helical structure the moments attain an equal value of $3.57(5)\mu_B$ and rotate normal to the propagation vector $k = (3/4, 3/4, 0)$. In the amplitude modulated structure the maximal moment value is $2.94(2)\mu_B$ and all moments point normal to k, along the $(1\bar{1}0)$ axis.

Neutron diffraction patterns contain also diffuse scattering. On cooling, the broad diffuse bump narrows, grows in intensity, and yields the Bragg $(3/4, 3/4, 0)$ peak near 2 K. We analyze these two features as a broad Lorentzian and a resolution-limited Gaussian. The temperature dependence of these components is also presented in Fig. 4(c). The two features reveal the long-range (LRO) and short-range (SRO) order in the sample, respectively. The narrow Gaussian Bragg peak dominates at low temperatures but then vanishes around 2 K, which is consistent with the low-T anomaly of the magnetic susceptibility (Fig. 3). It is a clear indicator of the LRO in $MnSc_2Se_4$ present below $T_{N1} = 2.04$ K. On the other hand, the Lorentzian contribution extends to higher temperatures and can be ascertained up to 18.4 K corresponding to $|\Theta_{CW}|$. Hence, these results substantiate that short-range correlations evolve below Θ_{CW} and even tend to persist around $T = 1.6$ K, but due to the frustration effects, the LRO is restrained down to $T_{N1} = \Theta_{CW}/10$.

IV. DYNAMIC MAGNETIC CORRELATIONS

Inelastic neutron scattering data were collected with the incident neutron wavelength of 5.75 Å ($E_i = 2.47$ meV) on

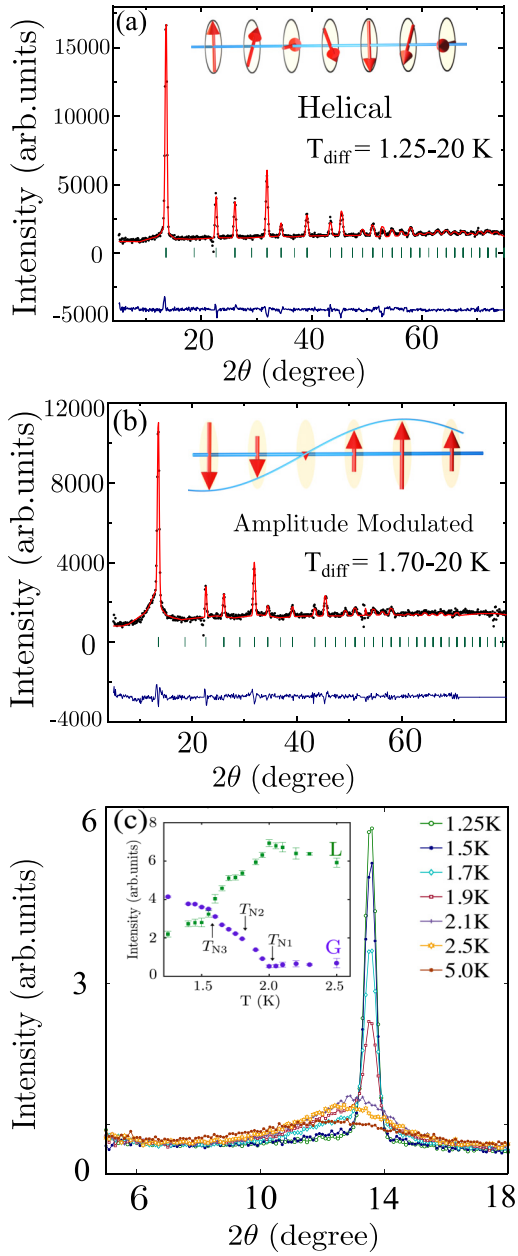

FIG. 4. (a), (b) Representative plots showing neutron powder diffraction refinement for the difference pattern obtained after subtracting the data at 20 K from low T and a constant has been added to prevent the negative intensities after the difference. Data points are shown by solid circles (black). The solid line indicates the calculated intensity (red), the vertical bars indicate the peak positions (green), and the bottom line (blue) shows the difference between the observed and the calculated intensity. (a) The refinement shown for the difference data fitted against the helical model and (b) for the amplitude modulated model. (c) Temperature evolution of the $(\frac{3}{4}\frac{3}{4}0)$ magnetic Bragg peak. Inset: Evolution of the Lorentzian (L) and the Gaussian (G) peak components.

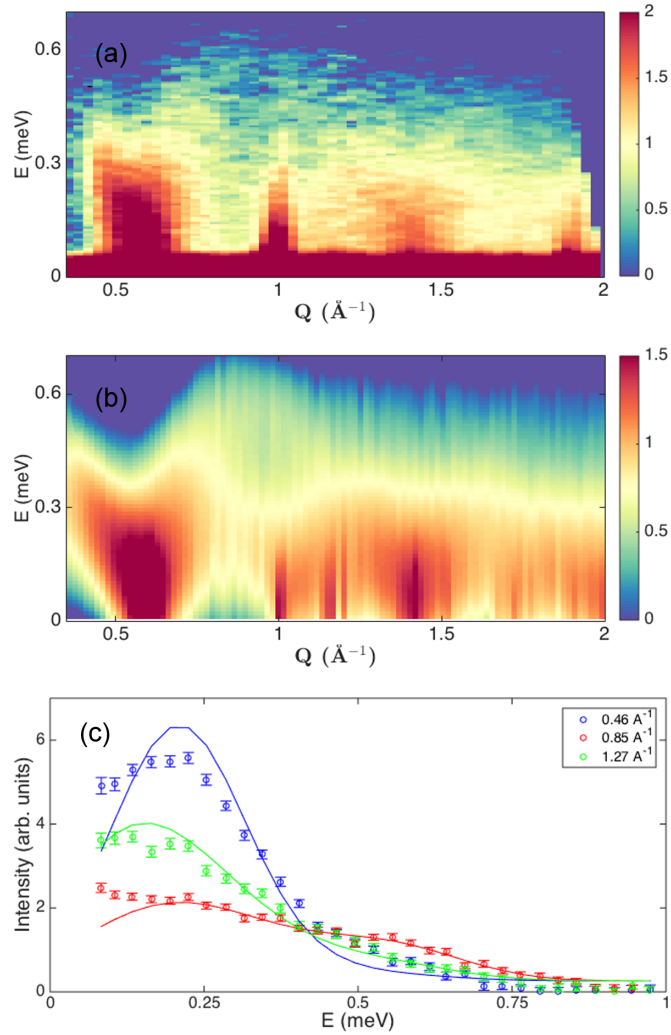

FIG. 5. (a) Experimental excitation spectrum measured on FOCUS with $E_i = 2.47$ meV at $T = 1.6$ K and (b) SPINW calculated spectrum for $J_1 = -0.24$ K, $J_2 = 0.37$ K, and $J_3 = 0.072$ K. (c) SPINW fit of three Q strips, $Q = 0.46$, 0.85, and 1.27 Å^{-1} summed over $\delta Q = 0.06$ Å^{-1}. Data binned with 0.03 meV are shown by circles, and solid lines indicate the calculated intensity.

the time-of-flight (TOF) spectrometer FOCUS, SINQ at PSI. For this experiment a ∼4.2 g powder sample was filled into an Al can of an inner diameter of 8 mm which was then cooled to $T = 1.6$ K, the base temperature of a He cryostat. For the data reduction, we employed the standard DAVE program [23], which converts the TOF data into energy transfers at constant Q. To account for the background, data for an empty Al can were subtracted. We observed spin-wave excitations at the base temperature of 1.6 K, emerging from the Bragg positions and reaching the energy maximum of 0.7 meV at $Q = 0.6$ Å^{-1} [see Fig. 5(a)].

To understand these excitations, we performed calculations based on the linear spin-wave theory using the SPINW package [24]. We used the J_1-J_2-J_3 model to fit the excitations at $Q = 0.46$, 0.85, and 1.27 Å^{-1} as shown in Fig. 5(c). These Q cuts contain the most pronounced features of the excitations—dispersive branches and the high-energy edge of the flat excitation band. The fitted parameters were the J_1 and J_3 exchange constants, the scale, and constant background. J_2 is related to J_1 and J_3 by the equation [6]

$$\frac{J_3}{|J_1|} = \frac{-1 + (4 - 2\sqrt{2})J_2/|J_1|}{4\sqrt{2} - 3}.$$

TABLE I. The experimental and theoretical information about the magnetic properties of the $MnSc_2X_4$ (X = S, Se) compounds.

	$MnSc_2S_4$	$MnSc_2Se_4$
Θ_{CW}	−22.9 K	−18.4 K
f	10	9
J_1	−0.31 K	−0.24 K
J_2	0.46 K	0.37 K
J_3	0.087 K	0.072 K
J_2/J_1	1.48	1.52

The best-fitted parameters are found to be $J_1 = -0.24$ K, $J_2 = 0.37$ K, and $J_3 = 0.072$ K.

The ratio of $J_2/|J_1|$ for $MnSc_2Se_4$ lies in the regime of the highly frustrated system as the threshold to realize the spiral spin-liquid state is given by $J_2/|J_1| > 1/8$ [1]. The values of the exchange parameters J_2 and J_3 are significantly smaller and J_1 is nearly similar, relative to the sulfur analog [7] (see Table I). These results can be understood intuitively by addressing the effect of the larger size of the Se^{2-} ion and, as a consequence, the strength of the exchange interactions weakens. The knowledge of the rearrangement of electronic bands and the covalency effect which contribute to the moment formation and exchange would allow a deeper comprehension. The fitting results reflect that the substitution of the X ion (S → Se) in $MnSc_2X_4$ reduces the energy window of excitations for $MnSc_2Se_4$ (Fig. 5).

V. SUMMARY AND DISCUSSION

To summarize, using neutron scattering and macroscopic magnetic magnetic measurements, we unravel the complex magnetism of the $MnSc_2Se_4$ compound. The macroscopic magnetization data infer multiple long-range order transitions at temperatures which are by nearly one order of magnitude smaller than the Curie-Weiss temperature of 18.4 K, indicating significant frustration. Our neutron powder diffraction studies identify the long-range order as associated with the propagation vector $k = (3/4, 3/4, 0)$.

At 1.25 K we reveal the helical magnetic order, at 1.7 K—the amplitude modulated one alike in the sister compound $MnSc_2S_4$. Yet, no incommensurate phase was detected. In addition to the long-range order we found short-range correlations manifested as diffuse scattering, that in the 1.8 K $< T <$ 2 K range coexists with magnetic Bragg peaks and persists towards high temperatures. Presumably this diffuse feature is the powder averaged surface of spiral propagation vectors in analogy to $MnSc_2S_4$ [8,11]. Thus, $MnSc_2Se_4$ undergoes multiple transitions from a high-T uncorrelated state for $T \geqslant |\Theta_{CW}|$, via the spin-liquid state for the temperatures between, $T_N \leqslant T \leqslant |\Theta_{CW}|$, to magnetically long-range ordered states for $T \leqslant T_N$.

Our inelastic neutron scattering results, fitted to the J_1-J_2-J_3 model, allowed us to determine the exchange parameters for $MnSc_2Se_4$. The obtained ratio of J_2/J_1 suggests that the $MnSc_2Se_4$ compound is another example of the A-site spinel, where the spiral spin-liquid state is realized. Additionally, we suggest that a deeper insight on the magnetic anisotropy and the H-T phase diagram can be obtained with the single-crystalline samples. Such exploration can be helpful to understand the topological nontrival skyrmions discovered in such systems. Our present study unravels a potential candidate from the family of A-site spinels to host these states.

ACKNOWLEDGMENTS

This work was performed at SINQ, Paul Scherrer Institute, Villigen, Switzerland with a financial support of the Swiss National Science Foundation (Grant No. 200020-182536). This work was partly supported by the Deutsche Forschungsgemeinschaft (DFG) through Transregional Research Collaboration TRR 80 (Augsburg, Munich, and Stuttgart), and by the project ANCD 20.80009.5007.19 (Moldova). We thank S. Gao and S. Nikitin for their help in the analysis of the neutron spectra with SPINW and S. Ghara and D. S. Negi for the useful discussions.

[1] D. Bergman, J. Alicea, E. Gull, S. Trebst, and L. Balents, Nat. Phys. **3**, 487 (2007).
[2] A. P. Schnyder, S. Ryu, and A. W. W. Ludwig, Phys. Rev. Lett. **102**, 196804 (2009).
[3] S. Ryu, Phys. Rev. B **79**, 075124 (2009).
[4] C. Wang, A. Nahum, and T. Senthil, Phys. Rev. B **91**, 195131 (2015).
[5] G. Chen, Phys. Rev. B **96**, 020412(R) (2017).
[6] S. B. Lee and L. Balents, Phys. Rev. B **78**, 144417 (2008).
[7] S. Gao, H. D. Rosales, F. A. G. Albarracín, V. Tsurkan, G. Kaur, T. Fennell, P. Steffens, M. Boehm, P. Čermák, A. Schneidewind, E. Ressouche, D. C. Cabra, C. Rüegg, and O. Zaharko, Nature (London) **586**, 37 (2020).
[8] S. Gao, O. Zaharko, V. Tsurkan, Y. Su, J. S. White, G. S. Tucker, B. Roessli, F. Bourdarot, R. Sibille, D. Chernyshov, T. Fennell, A. Loidl, and C. Rüegg, Nat. Phys. **13**, 157 (2017).
[9] T. Suzuki, H. Nagai, M. Nohara, and H. Takagi, J. Phys.: Condens. Matter **19**, 145265 (2007).
[10] N. Tristan, J. Hemberger, A. Krimmel, H.-A. K. von Nidda, V. Tsurkan, and A. Loidl, Phys. Rev. B **72**, 174404 (2005).
[11] A. Krimmel, M. Mücksch, V. Tsurkan, M. M. Koza, H. Mutka, C. Ritter, D. V. Sheptyakov, S. Horn, and A. Loidl, Phys. Rev. B **73**, 014413 (2006).
[12] A. Krimmel, H. Mutka, M. M. Koza, V. Tsurkan, and A. Loidl, Phys. Rev. B **79**, 134406 (2009).
[13] H. S. Nair, Z. Fu, J. Voigt, Y. Su, and Th. Brückel, Phys. Rev. B **89**, 174431 (2014).
[14] J. G. MacDougall, D. Gout, J. L. Zarestky, G. Ehlers, A. Podlesnyak, M. A. McGuire, D. Mandrus, and S. E. Nagler, Proc. Natl. Acad. Sci. USA **108**, 15693 (2011).
[15] V. Fritsch, J. Hemberger, N. Büttgen, E.-W. Scheidt, H.-A. Krug von Nidda, A. Loidl, and V. Tsurkan, Phys. Rev. Lett. **92**, 116401 (2004).

[16] P. G. Radaelli, Y. Horibe, M. J. Gutmann, H. Ishibashi, C. H. Chen, R. M. Ibberson, Y. Koyama, Y.-S. Hor, V. Kiryukhin, and S.-W. Cheong, Nature (London) **416**, 155 (2002).

[17] K. W. Plumb, J. R. Morey, J. A. Rodriguez-Rivera, H. Wu, A. A. Podlesnyak, T. M. McQueen, and C. L. Broholm, Phys. Rev. X **6**, 041055 (2016).

[18] A. Biffin, Ch. Rüegg, J. Embs, T. Guidi, D. Cheptiakov, A. Loidl, V. Tsurkan, and R. Coldea, Phys. Rev. Lett. **118**, 067205 (2017).

[19] A. N. Yaresko, Phys. Rev. B **77**, 115106 (2008).

[20] J. Rodríguez-Carvajal, Phys. B: Condens. Matter **192**, 55 (1993).

[21] T. Ngo, Balance between thermopower, electric and magnetic interactions in $CuCrO_2$, $Bi_8Rh_7O_{22}$ and $MnSc_2Se_4$, Ph.D. thesis, University of Groningen, 2015.

[22] L. Pawlak and M. Duczmal, Int. J. Mod. Phys. B **07**, 1020 (1993).

[23] R. T. Azuah, L. R. Kneller, Y. Qiu, P. L. W. Tregenna-Piggott, C. M. Brown, J. R. D. Copley, and R. M. Dimeo, J. Res. Natl. Inst. Stand. Technol. **114**, 341 (2009).

[24] S. Toth and B. Lake, J. Phys.: Condens. Matter **27**, 166002 (2015).